Spectrochimica Acta Part A: Molecular and Biomolecular Spectroscopy 246 (2021) 119059

Contents lists available at ScienceDirect

Spectrochimica Acta Part A: Molecular and Biomolecular Spectroscopy

journal homepage: www.elsevier.com/locate/saa

Design, synthesis and application of a dual-functional fluorescent probe for reactive oxygen species and viscosity

Hongyu Li [a,b], Ya Liu [a,b], Xiaoyi Li [a], Xiaohua Li [a,*], Huimin Ma [a,b]

[a] Key Laboratory of Analytical Chemistry for Living Biosystems, Institute of Chemistry, Chinese Academy of Sciences, Beijing 100190, China
[b] University of Chinese Academy of Sciences, Beijing 100049, China

ARTICLE INFO

Article history:
Received 25 May 2020
Received in revised form 10 September 2020
Accepted 6 October 2020
Available online 09 October 2020

Keywords:
NIR
Fluorescent probe
Viscosity
Hypochlorous acid (OCl^-)
Peroxynitrite ($ONOO^-$)
Cell imaging

ABSTRACT

A fluorescence probe based on cyanine fluorophore was designed and synthesized in this work, which can be used to determine viscosity and reactive oxygen species (e.g., OCl^-, $ONOO^-$) at different wavelengths. Under a low viscosity medium, the fluorescence quantum yield of the probe is very low; however, with the increase of the medium viscosity, the probe's emission at 571 nm is enhanced by nearly 25-fold due to the inhibition of intramolecular rotations. On the other hand, the probe shows a rapid and linear fluorescence response at 710 nm to OCl^- or $ONOO^-$ within 1 min. The different spectral response regions of the probe permit the selective detection of both viscosity and reactive oxygen species. Furthermore, the probe is demonstrated to be cell permeable and capable of detecting the viscosity and the total amount of OCl^-/$ONOO^-$ in living cells with the help of confocal microscope fluorescence imaging.

1. Introduction

Cell viscosity is a very important physiological parameter, which is related to various diffusion-mediated cellular processes, including the transmission of substances, the interaction between biological molecules, and the diffusion of metabolites. In general, the cytoplasmic viscosity of normal cells is about 1–2 cP, which however is significantly enhanced to 140 cP or even higher in abnormal conditions [1–4]. These changes in intracellular viscosity are associated with many diseases [5–11], such as diabetes, hypertension, high cholesterol, arteriosclerosis and malignant tumors.

Reactive oxygen species (ROS), i.e., hypochlorous acid (OCl^-), peroxynitrite ($ONOO^-$), hydrogen peroxide (H_2O_2), superoxide anion radical ($O_2^{\bullet-}$), hydroxyl radical (•OH), nitric oxide (NO) and singlet oxygen ($^1O_2$), etc., are a series of substances with high oxidative reactivity, which are also characterized by low concentration and short life span. Among these ROS, OCl^-, produced by the reaction of H_2O_2 and Cl^- under the catalysis of myeloperoxidase (MPO) [12], has been proved to play an important role in killing multiple pathogens [13]; $ONOO^-$, generated in the presence of NO and $O_2^{\bullet-}$ [14], possesses strong oxidation and nitration ability and has crucial function in cell signaling [15]. Therefore, regulation of ROS production is of great significance for maintaining cellular immunity as well as many other functions.

To date, various fluorescent probes have been developed for detecting ROS [16–18] and cellular viscosity [19–25], respectively. However, evidence has suggested that ROS might be associated with the change of intracellular viscosity [19,26]. Thus, simultaneous detection of these two parameters is of great importance for studies of various physiological processes such as apoptosis. Unfortunately, dual-functional fluorescent probes with the capacity of detecting viscosity and ROS are rather rare [19,26]. Hence, the development of such a dual-functional fluorescent probe is very necessary.

Herein, a cyanine-based dual-functional fluorescent probe (**CBRV**, see Scheme 1) is reported for the detection of ROS and viscosity. As depicted in Scheme 1A, **CBRV** possesses two small π-conjugations with two positive charges, thus exhibiting short absorption and emission wavelengths. In addition, a phenylboronate ester group is appended to the fluorophore (**CRV**) for the recognition of ROS (such as OCl^-, $ONOO^-$ and H_2O_2) [27–30]; the oxidation of the phenylboronate ester results in the generation of a larger polymethine π-conjugation system via electron rearrangement and eventually the NIR fluorescence off-on response at 710 nm. This NIR fluorescence is beneficial to eliminating the short wavelength background fluorescence from bio-samples and thus achieving a sensitive detection. On the other hand, the typical molecular rotor feature of **CBRV** is conducive to the detection of viscosity (Scheme 1B). With the increase of environmental viscosity, the intramolecular rotation of rotatable vinyl bond is restricted, and thus the twisted intramolecular charge transfer (a non-radiative process) is inhibited [31], resulting in fluorescence

* Corresponding author.
E-mail address: lixh@iccas.ac.cn (X. Li).

https://doi.org/10.1016/j.saa.2020.119059
1386-1425/

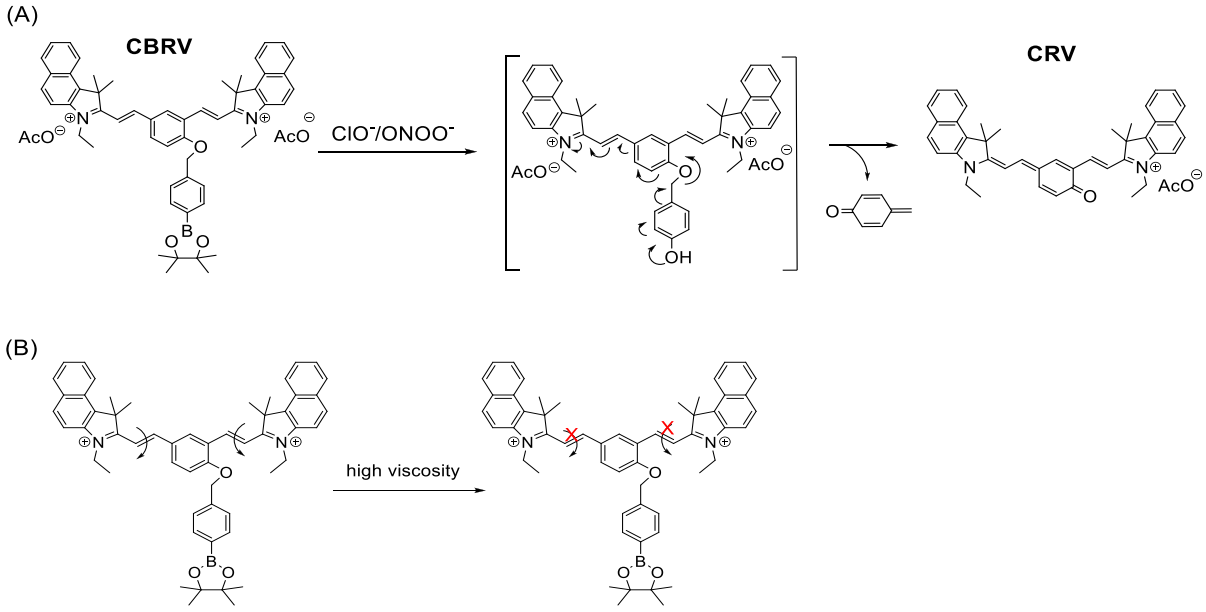

Scheme 1. Response mechanism of **CBRV** to OCl^-/$ONOO^-$ (A) and viscosity (B).

enhancement of **CBRV** at 571 nm, which allows independent detection of viscosity in a channel different from ROS.

2. Experimental section

2.1. Materials and instruments

4-Hydroxymethylphenylboronic acid pinacol ester was purchased from Beijing innochem Science&Technology Co., Ltd. 1,1,2-Trimethyl-1H-benzo[*e*]indole and 4-hydroxy-isophthal-aldehyde were obtained from Shanghai Aladdin Regent Co., Ltd. 3-(4,5-Dimethyl-2-thiazolyl)-2,5-diphenyl-2H-tetrazolium brominde (MTT), lipopolysaccharide (LPS), phorbol-12-myristate-13-acetate (PMA), and *N*-acetylcystine (NAC) were purchased from Sigma-Aldrich. Murine recombinant interferon-γ (IFN-γ) was obtained from ProSpec-Tany TechnoGene Ltd. The cell lines (HeLa and RAW264.7), Dulbecco's modified Eagle's media (DMEM), and RPMI 1640 media were purchased from KeyGEN Bio TECH Co., Ltd., Nanjing, China. The preparation and/or concentration determination of *tert*-butoxy radical (TBO•) and other reactive oxygen species (OCl^-, $ONOO^-$, H_2O_2, •OH, NO, TBHP) were made according to the literatures [32–34]. The stock solution (1 mM) of **CBRV** was prepared by dissolving in methanol. Ultrapure water (over 18 MΩ·cm) from a Milli-Q reference system (Millipore) was used throughout.

UV–vis absorption spectra were recorded by a TU-1900 spectrophotometer (Beijing, China) in 1 cm quartz cells and fluorescence spectra were determined on a Hitachi F-4600 spectrophotometer in 1 × 1 cm quartz cell with both excitation and emission slit widths of 10 nm. ^1H and ^{13}C NMR spectra were measured on Bruker Fourier-300 spectrometers. High-resolution electrospray ionization mass spectra (HR-ESI-MS) were performed on an APEX IVFTMS instrument (Bruker Daltonics). The incubation was carried out in a shaker water bath (SKY-100C, Shanghai Sukun Industry & Commerce Company). The absorbance for MTT analysis was recorded on a microplate reader (BIOTEK Synergy HT, USA) at 490 nm. Confocal fluorescence images were performed on a FV 1200-IX83 Confocal laser scanning microscope (Olympus, Japan). Image process was accomplished with Olympus software (FV10-ASW).

2.2. Synthesis of *CBRV* and characterization

CBRV was synthesized according to the route shown in Scheme S1 through four steps [35]. First, a powder of 1,1,2-trimethyl-1H-benzo [e] indole (compound **1**, 2.1 g, 10 mmol) and bromoethane (1 g, 10 mmol) in acetonitrile (10 mL) were heated under 100 °C to reflux for 12 h with stirring. After the reaction was completed, the solvent was evaporated under reduced pressure. The crude product was purified by silica gel chromatograghy (CH_2Cl_2/MeOH, 100:4, v/v), obtaining **2** as a grey-green solid.

Next, KI (2 mg, 12 mmol) and chlorotrimethylsilane (24 mL) were added slowly into 4-hydroxymethylphenylboronic acid pinacol ester (compound **3**, 0.8 g, 3.4 mmol) in anhydrous acetonitrile (30 mL) at 0 °C. After stirring at room temperature for 30 min, 10 mL of ethyl acetate was added, and then washed with saturated sodium thiosulfate to remove the excess potassium iodide. The organic phase was dried over anhydrous Na_2SO_4, evaporated under reduced pressure and subjected to silica gel chromatography (petroleum ether/ethyl acetate, 100:3, v/v), affording **4** as a white solid.

For compound **6** [30], 4-hydroxyisophthalaldehyde (**5**, 104 mg, 0.69 mmol) and K_2CO_3 (236 mg, 2.38 mmol) in anhydrous acetonitrile (15 mL) were stirred at 0 °C for 10 min. Then, compound **4** (260 mg, 0.76 mmol) was added and the mixture was stirred at room temperature overnight. The solvent was removed under reduced pressure to give **6** as a white solid, which was purified by silica gel chromatography (petroleum ether/ethyl acetate, 100:30, v/v).

Finally, to get our probe, compound **2** (80 mg, 0.2 mmol) and compound **6** (159 mg, 0.5 mmol) were dissolved in acetic anhydride (10 mL). The reaction mixture was refluxed for 3 h under 60 °C, and then the solvent was removed under reduced pressure. The resulting residue was purified by column chromatography on silica gel (CH_2Cl_2/methanol =100: 4, v/v) to afford **CBRV** as an orange powder (100 mg, yield 50.1%). The ^1H and ^{13}C NMR spectra of **CBRV** are shown in Figs. S1 and S2 in the Supporting Information, respectively. ^1H NMR δ (300 MHz, Methanol-d_4): 9.23 (s, 1H), 8.81–8.70 (d, 2H, J = 15.0 Hz), 8.47–8.40 (d, 3H, J = 12.0 Hz), 8.28–8.16 (s, 4H), 8.08–8.05 (s, 3H), 8.02–7.90 (d, 5H, J = 18.0 Hz), 7.84–7.59 (s, 5H), 5.51 (s, 2H), 5.00–4.95 (m, 2H, J = 9 Hz), 4.72–4.68 (m, 2H, J = 6 Hz), 2.18 (s, 6H), 2.08 (s, 6H), 1.73–1.68 (t, 3H, J = 6 Hz), 1.51–1.47 (t, 3H, J = 6 Hz),

1.39 (s, 12H). ^{13}C NMR δ (75 MHz, Methanol-d_4):182.9, 182.6, 162.8152.2, 147.4, 139.3, 138.8, 137.9, 136.6, 135.0, 134.5, 134.1, 134.0, 131.5, 131.4, 130.0, 128.8, 128.3, 128.3, 127.6, 127.4, 127.3, 127.2, 124.0, 122.9, 114.2, 113.7, 112.3, 110.8, 84.0, 54.3, 43.1, 42.8, 25.2, 25.2, 23.9, 23.6, 13.2, 13.0. HR-ESI-MS: *m/z* calcd for **CBRV** ($C_{55}H_{59}BN_2O_3^{2+}$, $[M]^{2+}$); 403.230846, found, 403.230902.

2.3. Preparation of ROS

As mentioned above, the preparation and concentration determination of ROS were made following the methods reported in literature [32–34,37,38], in which •OH was generated from the Fenton reaction of Fe^{2+} (10 μM) and H_2O_2 (100 μM).

2.4. General procedure for spectral measurements of ROS and viscosity

CBRV was dissolved in methanol to prepare its stock solution of 1 mM. Unless otherwise noted, all the spectral measurements were performed in 20 mM phosphate buffer (pH 7.4) according to the following procedure. A 3 mL of 20 mM phosphate buffer was added to a test tube, followed by addition of 30 μL **CBRV** stock solution (1 mM) and appropriate volume of reactant (OCl^-, $ONOO^-$ or other ROS and bioactive species) solution. After incubation with shaking at room temperature for 5 min, the absorption and fluorescence spectra were measured.

To test the effect of viscosity, 50 μL of the stock solution of **CBRV** was mixed with 5 mL of the methanol/glycerol mixture at different volume proportions in a test tube. The resulting solutions were shaken for 3 h and then cooled to room temperature. Afterwards, the absorption and fluorescence spectra of these solutions were measured at room temperature (25 °C).

2.5. Cytotoxicity assay

The cytotoxicity of **CBRV** to HeLa cells was examined by standard MTT assay [39].

2.6. Cell culture

RAW 264.7 cells (or HeLa cells) were cultured in RPMI 1640 media (DMEM) supplemented with 10% heat-inactivated new-born calf serum (fetal calf serum, FBS) in a humidified atmosphere of 95% air and 5% CO_2 at 37 °C.

2.7. Imaging endogenous ROS in cells

Cells (HeLa or RAW 264.7) were planted in glass bottom dishes, grown for 24 h and then treated with the stimulator (PMA or LPS/IFN-γ) for appropriate time. After that the cells were washed and incubated with 10 μM **CBRV** for 30 min, and fluorescence imaging was conducted with a 635 nm excitation source and emissions were collected from 670 to 750 nm. For elimination of ROS, HeLa cells were pretreated with PMA (10 nM) for 6 h, and RAW 264.7 cells were pretreated with LPS (1 μg/mL)/IFN-γ (100 ng/mL) for 15 h; then they were incubated for 1 h in the presence of NAC (1 mM), and finally washed by serum-free media and loaded with **CBRV** for 30 min before imaging.

2.8. Imaging endogenous viscosity in HeLa cells

HeLa cells were planted in glass bottom dishes, grown for 24 h and then treated with apoptotic agent (etoposide) for appropriate time. After that the cells were washed and incubated with 10 μM **CBRV** for 30 min for fluorescence imaging.

3. Results and discussion

3.1. Spectroscopic response of *CBRV* to ROS

The spectroscopic properties of **CBRV** are shown in Fig. 1 and Table S1. From the absorption and fluorescence spectra of **CBRV** before and after reaction with OCl^- or $ONOO^-$, it is seen that **CBRV** exhibits a strong absorption at 460 nm (Fig. 1A) and nearly no fluorescence (Fig. 1B). The reaction of **CBRV** with ROS produced a new absorption peak at 590 nm and a strong fluorescence emission at 710 nm, similar to that of the corresponding reaction product **CRV**. This supports the occurrence of the oxidative reaction, and the product **CRV** was further confirmed by mass spectral analyses (Fig. S4).

The effects of pH and reaction time on the reaction system were explored (Fig. S5A), revealing that **CBRV** functions well in the range of pH 6.0–9.0. On the other hand, the fluorescence increase of the reaction solution reached the maximum within 1 min (Fig. S5B). Thus, 5 min of the reaction time may be selected for this study.

Under the optimized conditions (reaction at pH 7.4 for 5 min), the linear relationship between **CBRV** and OCl^-/$ONOO^-$ concentration was investigated. As shown in Fig. 2A and C, the fluorescence intensity increases with increasing OCl^- or $ONOO^-$, and it is found that the fluorescence enhancement is directly proportional to the concentration of OCl^- and $ONOO^-$ in the range of 2–10 μM OCl^- and 2–16 μM $ONOO^-$, with a linear equation of $\Delta F = 44.09 \times C\ (\mu M) + 118$ ($R^2 = 0.99$) and $\Delta F = 37.80 \times C\ (\mu M) + 4.4 \times 10^{-10}93$ ($R^2 = 0.98$), respectively, where ΔF is the difference of fluorescence intensity of **CBRV** in the presence and absence of OCl^- or $ONOO^-$. The detection limits (3S/m, in which S is the standard deviation of blank measurements, n = 11, and m is the slope of the linear equation) are determined to be 128.8 nM and 150.2 nM, respectively.

Next, the selectivity of **CBRV** was studied for OCl^-/$ONOO^-$ over other potential ROS, including H_2O_2, •OH, NO, O_2•$^-$, TBHP and TBO•. As shown in Fig. S6, **CBRV** shows high selectivity to OCl^- or $ONOO^-$ over other ROS, except that H_2O_2 exhibits a moderate fluorescence response at higher concentrations, which, however, is a much slower reaction and lower intensity compared with that of OCl^- or $ONOO^-$ under the same optimal conditions (Fig. S5B). It is also noted that H_2O_2 and •OH produced similar signals (Fig. S6), which may be due to that the Fenton reaction is relatively slow under these conditions, and **CBRV** was mostly oxidized by H_2O_2. Moreover, the response of **CBRV** to inorganic salts and other bioactive substances, such as amino acids, and glucose, were also examined. As depicted in Fig. S7, the fluorescence of **CBRV** does not change significantly with the addition of these species. The above results.

indicated that **CBRV** showed relatively high selectivity for OCl^-/$ONOO^-$, which may be ascribed to the specific oxidation of **CBRV** by OCl^-/$ONOO^-$. In order to further investigate the selectivity of **CBRV**, the fluorescence of the oxidative product **CRV** was also examined in the presence of different ROS, inorganic salts and other bioactive substances. The results in Figs. S8 and S9 indicated that these interferences hardly caused fluorescence changes of **CRV**.

Further, the cytotoxicity of **CBRV** toward HeLa cells was studied by the MTT assay to test whether **CBRV** can be used for intracellular imaging. As shown in Fig. S10, **CBRV** at a high concentration of no more than 10 μM does not significantly damage the live cells, implying an excellent biocompatibility of **CBRV**. Furthermore, the fluorescence confocal imaging results (Fig. S11) suggested that **CRV** had good cellular permeability.

3.2. Response of *CBRV* to viscosity

Next, a series of tests on the fluorescence response of **CBRV** to different viscosities were made by mixing methanol/glycerol at different proportions. From Fig. 3A, it is seen that the emission maximum is at about 571 nm, and as the viscosity gradually increases from 0.59 cP (in pure methanol) to 945.35 cP (in pure glycerol) [22], the fluorescence is

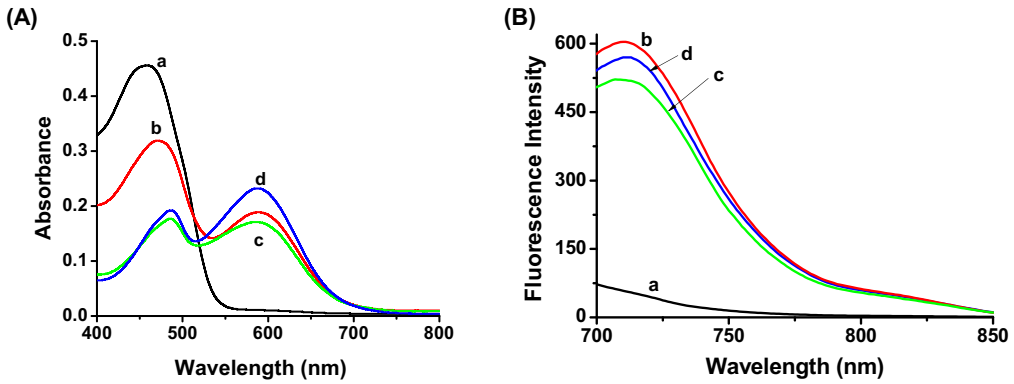

Fig. 1. (A) Absorption spectra of **CBRV** (10 μM) in phosphate buffer (pH 7.4) before (a) and after reaction with 10 μM of $ONOO^-$ (b) or OCl^- (c) for 5 min. (B) Fluorescence spectra of **CBRV** (10 μM) in phosphate buffer (pH 7.4) before (a) and after reaction with 10 μM of $ONOO^-$ (b) or OCl^- (c) for 5 min. $\lambda_{ex} = 485$ nm. The absorption and fluorescence spectra of **CRV** (10 μM) were given as curve (d) in Panels A and B, respectively.

enhanced largely, accompanied by a slight hypsochromic shift of the maximum wavelength. Furthermore, a good linearity is obtained between the fluorescence change and viscosity, which follows the Forster-Hoffmann equation [40,41] as Log $\Delta F = x \log \eta + c$ (where ΔF stands for the fluorescence change; η is the viscosity of solvent; x is probe-dependent constant and c is the constant related to **CBRV** concentration and temperature) with the x and c are 0.79 and 0.17 respectively. It should be pointed out that the correlation coefficient of the linear relationship is as high as 0.99, which indicates that **CBRV** may be of capable of monitoring the changes of viscosity.

In addition, pH and polarity of the solvent, which may often affect fluorescence response, were studied in detail. As shown in Fig. S12A, the fluorescence of **CBRV** is not much affected in the range of pH 6.0–7.4. In addition, the polarity effect of the solvent with different dielectric constants were also small (Fig. S12B). It should be noted that dichloromethane caused somewhat fluorescence response, which

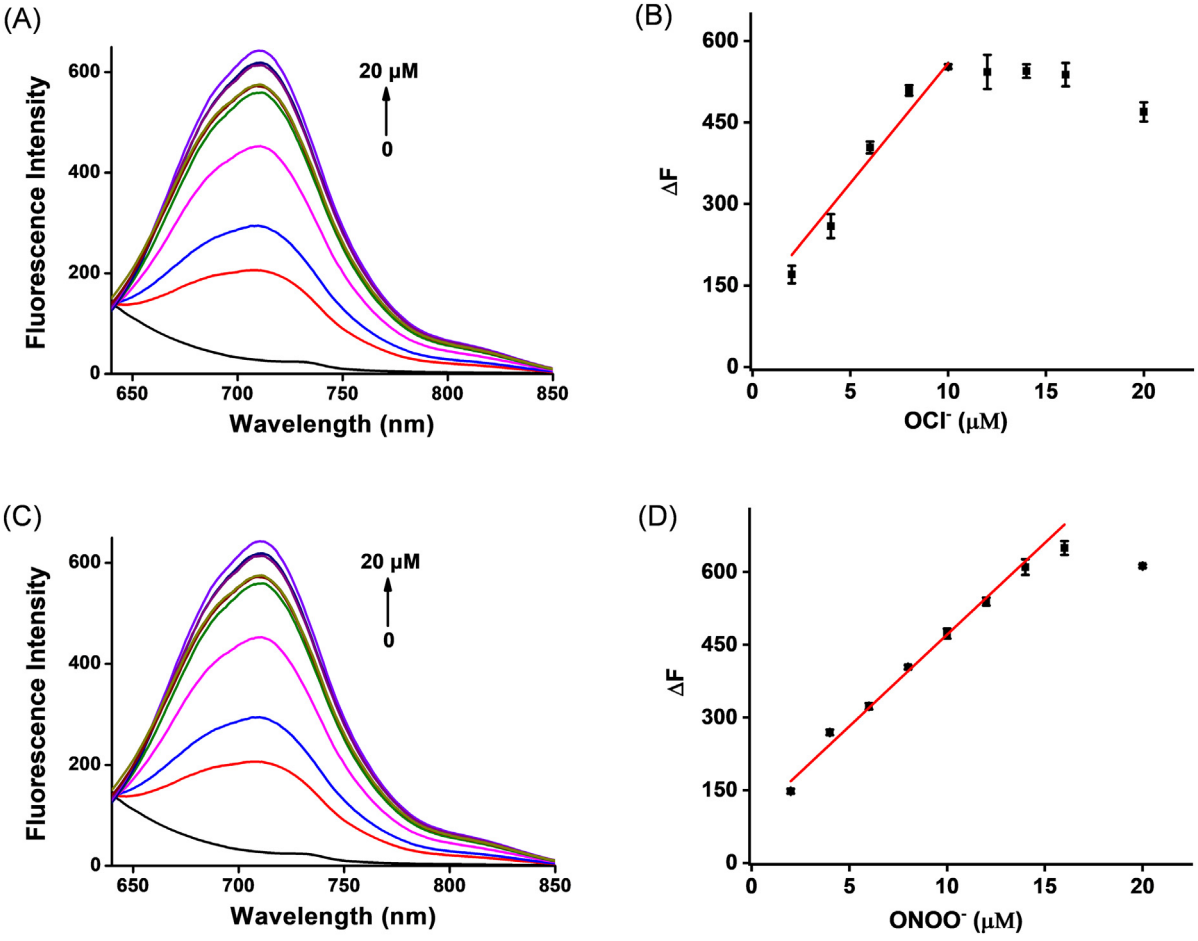

Fig. 2. Fluorescence responses of **CBRV** (10 μM) toward (A) OCl^- and (C) $ONOO^-$ at varied concentrations (0–20 μM) in phosphate buffer (pH 7.4). Linear fitting curves of ΔF against the concentration of (B) OCl^- and (D) $ONOO^-$. $\lambda_{ex}/\lambda_{em} = 485/710$ nm.

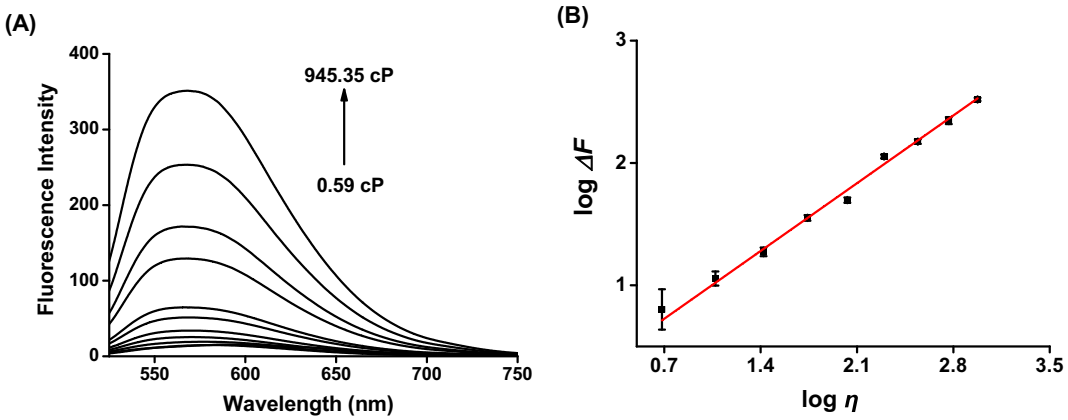

Fig. 3. (A) Fluorescence emission spectra of 10 μM **CBRV** in the mixture of varied ratios of methanol/glycerol (v/v) (from bottom to top): methanol only; 8:2; 7:3; 6:4; 5:5; 4:6; 3:7; 2:8; 1:9 and glycerol only. (B) The linearity between fluorescence change and viscosity. $\lambda_{ex/em}$ = 485/571 nm.

however is still smaller than 10% error in the fluorescence signal and could be neglected. Furthermore, the reversibility of **CBRV** in response to viscosity was examined. As shown in Fig. S13, **CBRV** exhibits good reversible fluorescence response to the variation of viscosity between 107 cP (methanol/glycerol, v/v = 6:4) and 26.4 cP (methanol/glycerol, v/v = 6:4). Thus, **CBRV** is suitable for monitoring the viscosity changes. Besides, we also tested the response of **CRV** to viscosity at 571 nm (viscosity channel) and 710 nm (ROS channel). As depicted in Fig. S14, **CRV** fluorescence is not sensitive to viscosity at 710 nm, meaning that the change of viscosity does not interfere with the detection of ROS. On the other hand, to check the possible influence of **CRV**, we measured the fluorescence change of **CBRV** by introducing **CRV**. The result (Fig. S15) showed that there was no significant interference from **CRV**. These observations indicated that our probe **CBRV** may serve as a dual-functional probe for the assay of ROS and viscosity.

3.3. Fluorescence imaging of ROS in cells

CBRV is a lipophilic cation, which implies that it might accumulate in cell mitochondria. To verify this possibility, a co-localization experiment

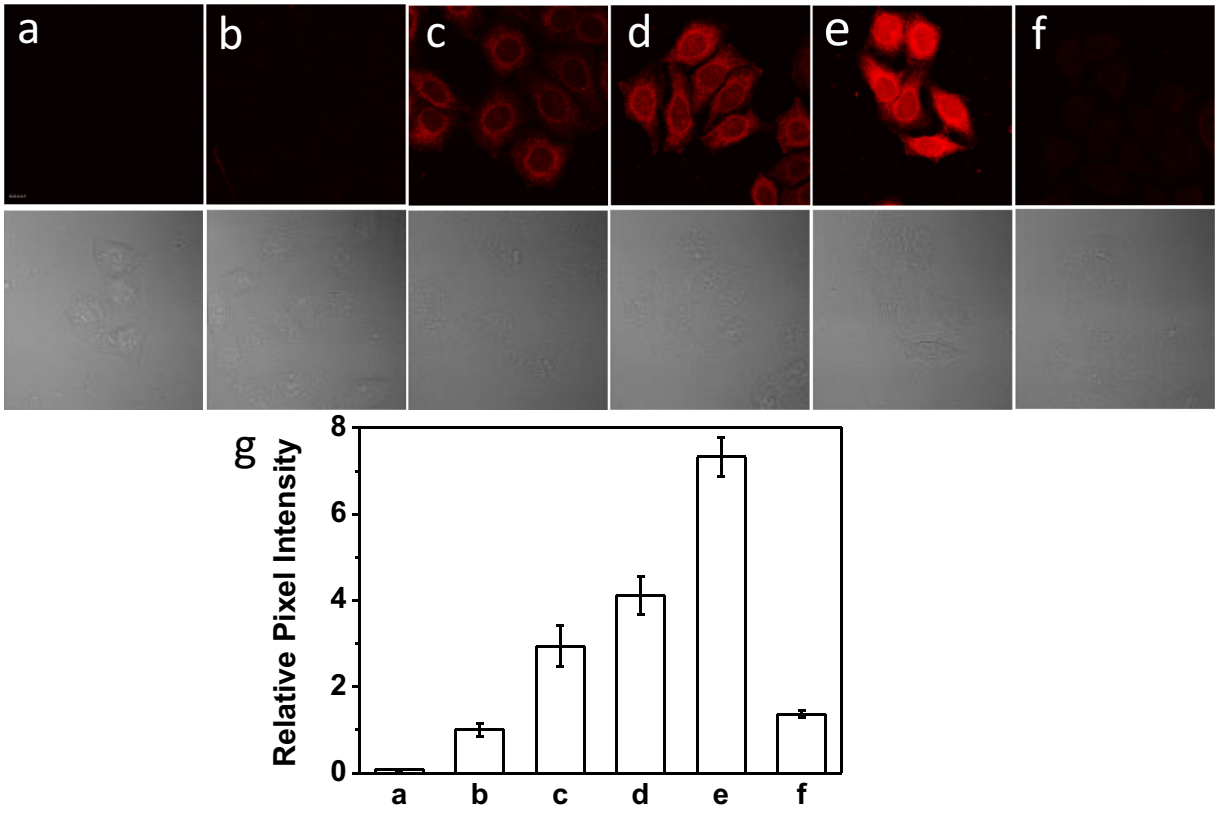

Fig. 4. Confocal fluorescence images of HeLa cells under different conditions. (a) Cells only. (b) Cells treated with **CBRV** (10 μM) for 30 min. (c–e) Cells pretreated with PMA (10 nM) for (c) 2 h, (d) 4 h and (e) 6 h, and then incubated with CBRV (10 μM) for 30 min. (f) Cells pretreated with PMA (10 nM) for 6 h, then incubated with NAC (1 mM) for 1 h, and finally incubated with CBRV (10 μM) for 30 min. The second row shows the corresponding differential interference contrast (DIC) images. λ_{ex} = 635 nm, λ_{em} = 670–750 nm. Scale bar: 10 μm. (g) Relative pixel intensity of fluorescence images a–f (the pixel intensity from image b is defined as 1.0). The results are presented as mean ± standard deviation (n = 3).

was performed. As shown in Fig. S16, the fluorescence from the Mito-red channel overlaps poorly with that from the **CBRV** channel, with a low Pearson's coefficient of 0.54, indicating that **CBRV** can be distributed in both cytosol and mitochondria of HeLa cells.

Next, to test whether **CBRV** could be used to detect the endogenous ROS change in cells, HeLa and RAW267.4 cells were selected as the cancer and macrophage model cells, respectively. HeLa cells were stimulated by PMA (10 nM) for different time, whereas RAW267.4 cells [42,43] were stimulated by LPS (1 μg/mL) and INF-γ(100 ng/mL) for 15 h; and then they were incubated with **CBRV** (10 μM) for another 30 min before subjected to fluorescence measurement. As shown in Fig. 4, the PMA-stimulated HeLa cells display gradually increased fluorescence with the extension of incubation time. Moreover, this enhancement can be greatly inhibited by NAC [44,45], suggesting the generation of ROS. Interestingly, similar results were observed in the PMA-stimulated RAW267.4 cells (Fig. S17). These data suggest that **CBRV** can be used for monitoring the production of the endogenous ROS in living cells.

3.4. Fluorescence imaging of viscosity in cells

Next, **CBRV** was attempted to measure the viscosity change in cells during apoptosis. Herein, HeLa cells with relatively large and well-defined morphology were chosen as the model cells, as well, which were incubated with **CBRV** (10 μM) for 30 min and then treated with 10 μM etoposide (an apoptotic agent) for different periods of time. As shown in Fig. 5, the fluorescence intensity (viscosity channel) of HeLa cells increases with the extension of time, accompanying an obvious contraction in terms of the contour morphology of cells, suggesting an increased degree of apoptosis, which may increase the viscosity of cells. This is consistent with our previous finding [26]. All these results indicate that **CBRV** could be applied to monitoring the viscosity change by fluorescence imaging.

4. Conclusion

In summary, we have developed **CBRV** as a new dual-functional fluorescent probe by conjugating a cyanine skeleton with a benzene boronic acid ester moiety. The probe exhibits high sensitivity and selectivity for OCl^-/$ONOO^-$ over other ROS, and good dual responses to both viscosity at around 571 nm and OCl^-/$ONOO^-$ at the NIR region of 710 nm. In addition, **CBRV** has been used to monitor the change of total ROS levels as well as the viscosity in living cells. The good analytical performance of **CBRV** may enable it to be applied to detection of OCl^-/$ONOO^-$ or viscosity in more biological samples.

CRediT authorship contribution statement

Hongyu Li: Methodology, Visualization, Investigation. **Ya Liu:** Writing - original draft, testing.

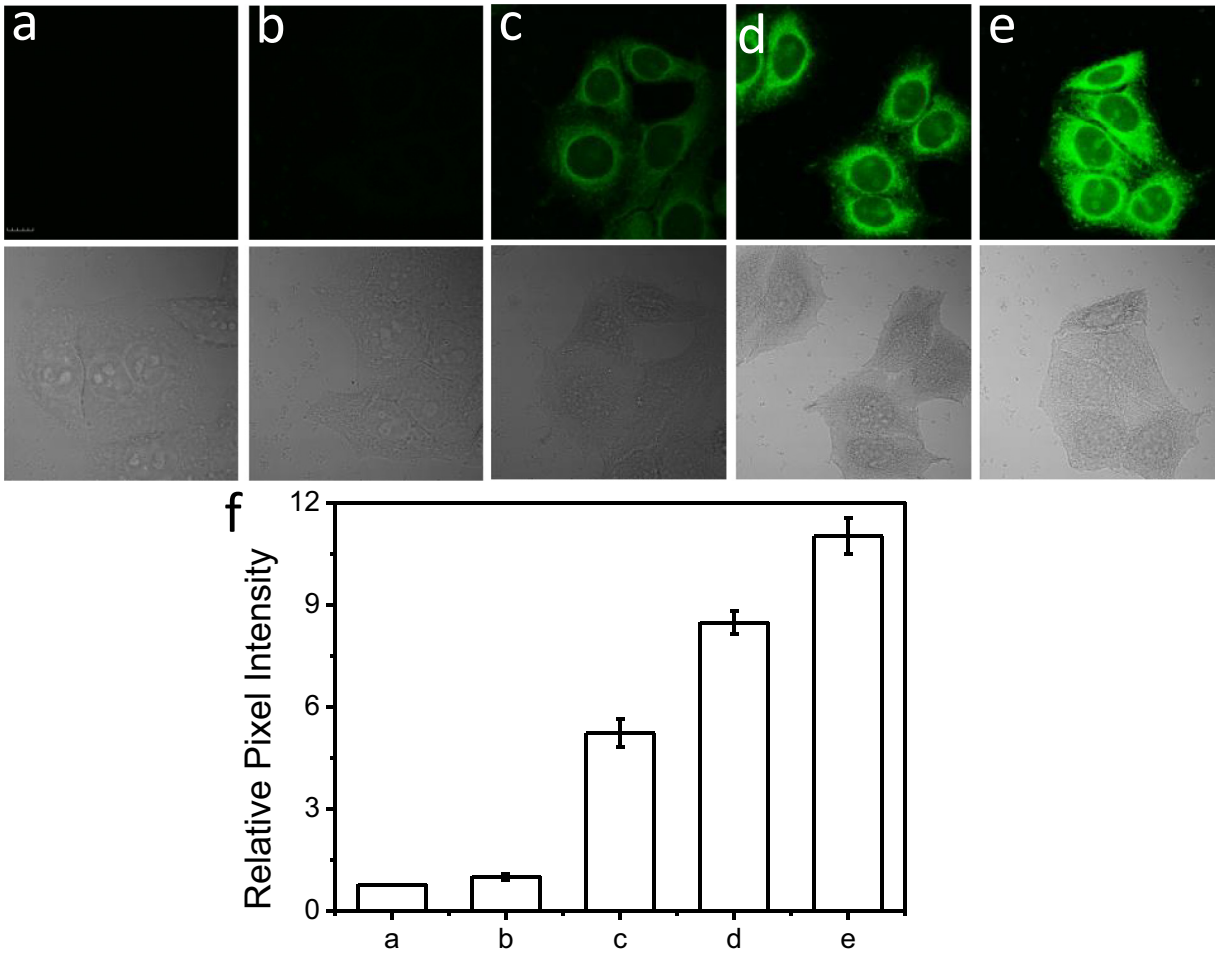

Fig. 5. Confocal fluorescence imaging of HeLa cells under different conditions. (a) Cells only. (b) Cells treated with **CBRV** (10 μM) for 30 min. Cells firstly treated with 10 μM etoposide for (c) 15 min, (d) 30 min, and (e) 45 min, respectively, and then incubated with **CBRV** for 30 min before imaging. The second row shows the corresponding DIC images. λ_{ex} = 488 nm, λ_{em} = 540–640 nm. Scale bar: 10 μm. (f) Relative pixel intensity of fluorescence images a–e (the pixel intensity from image b is defined as 1.0). The results are present as mean ± standard deviation (n = 3).

Xiaoyi Li: Testing and investigation. **Xiaohua Li:** Review & editing. **Huimin Ma:** Supervision, review & editing.

Declaration of competing interest

The authors declare that they have no known competing financial interests or personal relationships that could have appeared to influence the work reported in this paper.

Acknowledgment

We are grateful for the financial support from the NSF of China (Nos. 21775152, 22074151 and 21820102007).

Appendix A. Supplementary data

Supplementary data to this article can be found online at https://doi.org/10.1016/j.saa.2020.119059.

References

[1] M.K. Kuimova, S.W. Botchway, A.W. Parker, M. Balaz, H.A. Collins, H.L. Anderson, K. Suhling, P.R. Ogilby, Imaging intracellular viscosity of a single cell during photo-induced cell death, Nat. Chem. 1 (2009) 69–73, https://doi.org/10.1038/nchem.120.
[2] J.A. Dix, A.S. Verkman, Mapping of fluorescence anisotropy in living cells by ratio imaging. Application to cytoplasmic viscosity, Biophys. J. 57 (1990) 231–240, https://doi.org/10.1016/S0006-3495(90)82526-1.
[3] P.K. Luby, S. Mujumdar, R.B. Mujumdar, L.A. Ernst, W. Galbraith, A.S. Waggoner, Cytoarchitecture and physical properties of cytoplasm: volume, viscosity, diffusion, intracellular surface area, Biophys. J. 65 (1993) 236–242, https://doi.org/10.1016/S0074-7696(08)60527-6.
[4] M.K. Kuimova, G. Yahioglu, J.A. Levitt, K. Suhling, Molecular rotor measures viscosity of live cells via fluorescence lifetime imaging, J. Am. Chem. Soc. 130 (2008) 6672–6673, https://doi.org/10.1021/ja800570d.
[5] D.E. McMillan, Further observations on serum viscosity changes in diabetes mellitus, Metab. 31 (1982) 274–278, https://doi.org/10.1016/0026-0495(82)90064-6.
[6] G.B. Zhang, Y. Ni, D.T. Zhang, H. Li, N.X. Wang, C.M. Yu, L. Li, W. Huang, Rational design of NIR fluorescence probes for sensitive detection of viscosity in living cells, Spectrochim. Acta A 214 (2019) 339–347, https://doi.org/10.1016/j.saa.2019.02.068.
[7] M.A. Welte, Expanding roles for lipid droplets, Curr. Biol. 25 (2015) 470–481, https://doi.org/10.1016/j.cub.2015.04.004.
[8] M.F. Huang, L.N. Che, J.Y. Ning, W.L. Wu, X.D. He, J.Y. Miao, B.X. Zhao, A new lipid droplets-targeted fluorescence probe for specific detection of SO_2 derivatives in living cells, Sensors Actuators B Chem. 261 (2018) 196–202, https://doi.org/10.1016/j.snb.2018.01.139.
[9] G. Deliconstantinos, V. Villiotou, J.C. Stavrides, Modulation of particulate nitric oxide synthase activity and peroxynitrite synthesis in cholesterol enriched endothelial cell membranes, Biochem. Pharmacol. 49 (1995) 1589–1600, https://doi.org/10.1016/0006-2952(95)00094-G.
[10] P.K. Luby, Cytoarchitecture and physical properties of cytoplasm: volume, viscosity, diffusion, intracellular surface area, Int. Rev. Cytol. 192 (1999) 189–221, https://doi.org/10.1016/S0074-7696(08)60527-6.
[11] R.L. Letcher, S. Chien, T.G. Pickering, J.E. Sealey, J.H. Laragh, Direct relationship between blood pressure and blood viscosity in normal and hypertensive subjects: role of fibrinogen and concentration, Am. J. Med. 70 (1981) 1195–1202, https://doi.org/10.1016/0002-9343(81)90827-5.
[12] M. Sun, H. Yu, H. Zhu, F. Ma, S. Zhang, D. Huang, S. Wang, Oxidative cleavage-based near-infrared fluorescent probe for hypochlorous acid detection and myeloperoxidase activity evaluation, Anal. Chem. 86 (2014) 671–677, https://doi.org/10.1021/ac403603r.
[13] W.M. Nauseef, Myeloperoxidase in human neutrophil host defence, Cell. Microbiol. 16 (2014) 1146–1155, https://doi.org/10.1111/cmi.12312.
[14] R. Radi, A. Cassina, R. Hodara, C. Quijano, L. Castro, Peroxynitrite reactions and formation in mitochondria, Free Radic. Biol. Med. 33 (2002) 1451–1464, https://doi.org/10.1016/S0891-5849(02)01111-5.
[15] R.G. Allen, W.P. Lafuse, N.D. Powell, J.I. Marketon, L.T.M. Stiner-Jones, J.F. Sheridan, M.T. Bailey, Stressor-induced increase in microbicidal activity of splenic macrophages is dependent upon peroxynitrite production, Infect. Immun. 80 (2012) 3429–3437, https://doi.org/10.1128/IAI.00714-12.
[16] H. Meng, X.Q. Huang, Y. Lin, D.Y. Yang, Y.J. Lv, X.Q. Cao, G.X. Zhang, J. Dong, S.L. Shen, A new ratiometric fluorescent probe for sensing lysosomal HOCl based on fluorescence resonance energy transfer strategy, Spectrochim. Acta A 223 (2019) 117355, https://doi.org/10.1016/j.saa.2019.117355.
[17] X.X. Tang, H. Sun, J. Nie, X.E. Han, Y. Zhao, R. Zhang, Z.H. Ni, An o-hydroxyl aldehyde structure based naphthalimide derivative: reversible photochromic properties and its application in ClO- detection in living cells, Spectrochim. Acta A 219 (2019) 154–163, https://doi.org/10.1016/j.saa.2019.04.049.
[18] J.W. Hu, X. Zhang, T.T. Liu, H.W. Gao, S.L. Lu, K. Uvdal, Z. Hu, Ratiometric fluorogenic determination of endogenous hypochlorous acid in living cells, Spectrochim. Acta A 219 (2019) 232–239, https://doi.org/10.1016/j.saa.2019.04.024.
[19] X. Wang, F.L. Song, X.J. Peng, A versatile fluorescent probe for imaging viscosity and hypochlorite in living cells, Dyes Pigments 125 (2016) 89–94, https://doi.org/10.1016/j.dyepig.2015.10.012.
[20] K. Wang, W. Shi, J. Jia, S.M. Chen, H.M. Ma, Characterization of 2-phenylbenzo [g] quinoxaline derivatives as viscosity-sensitive fluorescent probes, Talanta 77 (2009) 1795–1799, https://doi.org/10.1016/j.talanta.2008.10.021.
[21] Y. Baek, S.J. Park, X. Zhou, G. Kim, H.M. Kim, A viscosity sensitive fluorescent dye for real-time monitoring of mitochondria transport in neurons, Biosens. Bioelectron. 86 (2016) 885–891, https://doi.org/10.1016/j.bios.2016.07.026i.
[22] Z.G. Yang, Y.X. He, J.H. Lee, N. Park, M. Sun, W.S. Chae, J.F. Cao, X.J. Peng, H. Jung, C. Kang, J.S. Kim, A self-calibrating bipartite viscosity sensor for mitochondria, J. Am. Chem. Soc. 135 (2013) 9181–9185, https://doi.org/10.1021/ja403851p.
[23] W. Sun, J.X. Cui, L.L. Ma, Z.L. Lu, B. Gong, L. He, R.B. Wang, Imaging nucleus viscosity and G-quadruplex DNA in living cells using a nucleus-targeting two-photon fluorescent probe, Analyst 143 (2018) 5799–5804https://doi.org/10.1039/C8AN01643G.
[24] X.L. Li, R.R. Zhao, Y. Wang, C.S. Huang, A new GFP fluorophore-based probe for lysosome labelling and tracing lysosomal viscosity in live cells, J. Mater. Chem. B 6 (2018) 6592–6598, https://doi.org/10.1039/C8TB01885E.
[25] M. Peng, J.L. Yin, W.Y. Lin, A two-photon fluorescent probe for detecting lipid droplet viscosity in living cells and zebra fish, New J. Chem. 42 (2018) 18521–18525, https://doi.org/10.1039/C8NJ04918A.
[26] H.Y. Li, X.H. Li, W. Shi, Y.M. Hu, Y. Fang, H.M. Ma, Ferroptosis is accompanied by •OH generation and cytoplasmic viscosity increase revealed via dual-functional fluorescence probe, J. Am. Chem. Soc. 141 (2019) 18301–18307, https://doi.org/10.1021/jacs.9b09722.
[27] Q. Xu, K. Lee, S. Lee, K.M. Lee, W. Lee, J. Yoon, A highly specific fluorescent probe for hypochlorous acid and its application in imaging microbe-induced HOCl production, J. Am. Chem. Soc. 135 (2013) 9944–9949, https://doi.org/10.1021/ja404649m.
[28] M.C.Y. Chang, A. Pralle, E.Y. Isacoff, C.J. Chang, A selective cell-permeable optical probe for hydrogen peroxide in living cells, J. Am. Chem. Soc. 126 (2004) 15392–15393, https://doi.org/10.1021/ja0441716.
[29] A. Sikora, J. Zielonka, M. Lopez, J. Joseph, B. Kalyanaraman, Direct oxidation of boronates by peroxynitrite: mechanism and implications in fluorescence imaging of peroxynitrite, Free Radic. Biol. Med. 47 (2009) 1401–1407, https://doi.org/10.1016/j.freeradbiomed.2009.08.006.
[30] N. Karton-Lifshin, E. Segal, L. Omer, M. Portnoy, R. Satchi-Fainaro, D.A. Shabat, A unique paradigm for a turn-on near-infrared cyanine-based probe: noninvasive intravital optical imaging of hydrogen peroxide, J. Am. Chem. Soc. 133 (2011) 10960–10965, https://doi.org/10.1021/ja203145v.
[31] M.S.A. Abdel-Mottaleb, R.O. Loutfy, R. Lapouyade, Non-radiative deactivation channels of molecular rotors, J. Photochem. Photobiol. A 48 (1989) 87–93, https://doi.org/10.1016/1010-6030(89)87093-5.
[32] X.H. Li, G.X. Zhang, H.M. Ma, D.Q. Zhang, J. Li, D.B. Zhu, 4, 5-Dimethylthio-4′-[2-(9-anthryloxy) ethylthio] tetrathia-fulvalene, a highly selective and sensitive chemiluminescence probe for singlet oxygen, J. Am. Chem. Soc. 126 (2004) 11543–11548, https://doi.org/10.1021/ja0481530.
[33] G.W. Chen, F.L. Song, J.Y. Wang, Z.G. Yang, S.G. Sun, J.L. Fan, X.X. Qiang, X. Wang, B.R. Dou, X.J. Peng, FRET spectral unmixing: a ratiometric fluorescent nanoprobe for hypochlorite, Chem. Commun. 48 (2012) 2949–2951, https://doi.org/10.1039/C2CC17617C.
[34] S.R. Liu, S.P. Wu, Hypochlorous acid turn-on fluorescent probe based on oxidation of diphenyl selenide, Org. Lett. 15 (2013) 878–881, https://doi.org/10.1021/ol400011u.
[35] E. Sella, D. Shabat, Dendritic chain reaction, J. Am. Chem. Soc. 131 (2009) 9934–9936, https://doi.org/10.1021/ja903032t.
[37] J. Zhou, L.H. Li, W. Shi, X.H. Gao, X.H. Li, H.M. Ma, HOCl can appear in the mitochondria of macrophages during bacterial infection as revealed by a sensitive mitochondrial-targeting fluorescent probe, Chem. Sci. 6 (2015) 4884–4888, https://doi.org/10.1039/C5SC01562F.
[38] R.M. Uppu, Synthesis of peroxynitrite using isoamyl nitrite and hydrogen peroxide in a homogeneous solvent system, Anal. Biochem. 354 (2006) 165–168, https://doi.org/10.1016/j.ab.2005.11.003.
[39] Q.Q. Wan, W. Shi, L.H. Li, H.M. Ma, Lysosomal pH rise during heat shock monitored by a lysosome-targeting near-infrared ratiometric fluorescent probe, Angew. Chem. Int. Ed. 53 (2014) 10916–11100, https://doi.org/10.1002/anie.201405742.
[40] M.A. Haidekker, E.A. Theodorakis, Environment-sensitive behavior of fluorescent molecular rotors, J. Biol. Eng. 4 (2010) 11–24, https://doi.org/10.1186/1754-1611-4-11.
[41] T. Förster, D.G. Hoffmann, Viskositätsabhängigkeit der Fluoreszenzquantenausbeuten einiger Farbstoffsysteme, Z. Phys. Chem. 75 (1971) 63–76, https://doi.org/10.1524/zpch.1971.75.1_2.063.
[42] J. Zielonka, M. Zielonka, A. Sikora, J. Adamus, J. Joseph, M. Hardy, O. Ouari, B.P. Dranka, B. Kalyanaraman, Global profiling of reactive oxygen and nitrogen species in biological systems: high-throughput real-time analyses, J. Biol. Chem. 287 (2012) 2984–2995, https://doi.org/10.1074/jbc.M111.309062.
[43] S.O. Lee, S.G. Lee, C.R. Brownmiller, H.W. Kang, Anti-inflammatory and antioxidant effects of anthocyanins of trifolium pratense (red clover) in lipopolysaccharide-stimulated raw-267.4 macrophages, Nutrients 12 (2020), 1089, https://doi.org/10.3390/nu12041089.
[44] K. Ishikawa, K. Takenaga, M. Akimoto, N. Koshikawa, A.H. Yamaguchi, K. Imanishi, Y. Nakada, J.I. Honma, Hayashi, ROS-generating mitochondrial DNA mutations can regulate tumor cell metastasis, Science 320 (2008) 661–664, https://doi.org/10.1126/science.1156906.
[45] L. Wu, I.C. Wu, C.C. DuFort, M.A. Carlson, X. Wu, L. Chen, C.T. Kuo, Y. Qin, J. Yu, S.R. Hingorani, D.T. Chiu, Photostable ratiometric pdot probe for in vitro and in vivo imaging of hypochlorous acid, J. Am. Chem. Soc. 139 (2017) 6911–6918, https://doi.org/10.1021/jacs.7b01545.